

## THE LOCAL SPACE DENSITY OF OPTICALLY SELECTED CLUSTERS OF GALAXIES

D. A. BRAMEL, R. C. NICHOL, AND A. C. POPE

Department of Physics, Carnegie Mellon University, 5000 Forbes Avenue, Pittsburgh, PA 15213

Received 1999 December 8; accepted 1999 December 14

### ABSTRACT

We present here new results on the space density of rich, optically selected clusters of galaxies at low redshift ( $z < 0.15$ ). These results are based on the application of the matched filter cluster-finding algorithm to  $1067 \text{ deg}^2$  of the Edinburgh/Durham Southern Galaxy Catalogue (EDSGC). This is the first major application of this methodology at low redshift, and in total we have detected 2109 clusters above a richness cutoff of  $R_m \geq 50$  (or  $\Lambda_{\text{cl}} \geq 10$ ). This new catalog of clusters is known as the Edinburgh/Durham Cluster Catalogue II (or EDCCII). We have used extensive Monte Carlo simulations to define the detection thresholds for our algorithm, to measure the effective area of the EDCCII, and to determine our spurious detection rate. These simulations have shown that our detection efficiency is strongly correlated with the presence of large-scale structure in the EDSGC data. We believe this is due to the assumption of a flat, uniform background in the matched filter algorithm. Using these simulations, we are able to compute the space density of clusters in this new survey. We find  $83.5^{+193.2}_{-36.9} \times 10^{-6} h^{-3} \text{ Mpc}^{-3}$  for  $100 \leq R_m < 200$  ( $\Lambda_{\text{cl}} \simeq 20$ ) systems,  $10.1^{+11.3}_{-4.3} \times 10^{-6} h^{-3} \text{ Mpc}^{-3}$  for  $200 \leq R_m < 400$  ( $\Lambda_{\text{cl}} \simeq 40$ ) systems, and  $2.3^{+2.5}_{-2.3} \times 10^{-6} h^{-3} \text{ Mpc}^{-3}$  for  $R_m > 400$  ( $\Lambda_{\text{cl}} > 80$ ) systems. These three richness bands roughly correspond to Abell richness classes 0, 1, and  $\geq 2$ , respectively. These new measurements of the local space density of clusters are in agreement with those found at higher redshift ( $0.2 < z_{\text{est}} < 0.6$ ) in the Palomar Distant Cluster Survey (PDCS) and therefore remove one of the major uncertainties associated with the PDCS as it had previously detected a factor of  $5 \pm 2$  more clusters at high redshift than expected compared to the space density of low-redshift Abell clusters. This discrepancy is now lessened and, at worst, is only a factor of  $4^{+10}_{-4}$ . This result illustrates the need to use the same cluster-finding algorithm at both high and low redshift to avoid such apparent discrepancies. We also confirm that the space density of clusters remains nearly constant out to  $z \sim 0.6$  in agreement with previous optical and X-ray measurements of the space density of clusters. Finally, we have compared the EDCCII with the Abell catalog. We detect nearly 60% of all Abell clusters in the EDCCII area regardless of their Abell richness and distance classes. For clusters in common between the two surveys, we find no strong correlation between the two richness estimates. In comparison,  $\sim 90\%$  of the EDCCII systems are new, although a majority of them have a richness lower than an Abell richness class of 0 and therefore would be below Abell's original selection criteria. However, we do detect 143 new clusters with  $R_m \geq 100$  (which corresponds to a richness class of greater than, or equal to, zero) that are not in the Abell catalog, i.e., 63% of the rich EDCCII systems. These numbers lend credence to the idea that the Abell catalog may be incomplete, especially at lower richnesses.

*Subject headings:* cosmology: observations — galaxies: clusters: general — galaxies: evolution — surveys

### 1. INTRODUCTION

Clusters of galaxies play a key role in tracing the distribution and evolution of mass in the universe (see, for example, Guzzo et al. 1992; Postman, Huchra, & Geller 1992; Nichol et al. 1992; Dalton et al. 1992; Bahcall & Soneira 1983; Reichart et al. 1999). Until recently, such studies have been based on catalogs of clusters constructed from visual scans of photographic plates, e.g., the Abell catalog (Abell 1958; Gunn, Hoessel, & Oke 1986; Abell, Corwin, & Olowin 1989; Couch et al. 1991). However, during the past decade there has been considerable progress in the construction of automated catalogs of clusters and groups that possess objective selection criteria. Such work includes cluster catalogs selected from digitized photographic material (Dodd & MacGillivray 1986; Lumsden et al. 1992; Dalton et al. 1994), from X-ray surveys (Kowalski et al. 1984; Ebeling et al. 1997; de Grandi et al. 1999; Gioia et al. 1990; Nichol et al. 1997, 1999; Rosati et al. 1998; Burke et al. 1997; Jones et al. 1998; Romer et al. 1999), and from large-area optical CCD surveys (Postman et al. 1996; Lidman & Peterson 1996; Zaritsky et al. 1997; Olsen et al. 1999).

There has also been great progress in the development of new cluster-finding algorithms. The first automated cluster catalogs used simple variants on the “peak-finding” algorithm (Lumsden et al. 1992) or the percolation method (Dalton et al. 1994). In recent years, several new, more sophisticated algorithms have become available, including the matched filter algorithm—in several different flavors (Postman et al. 1996; Kawasaki et al. 1998; Kepner et al. 1999; Schuecker & Boehringer 1998)—the wavelet filter (Slezak, Bijaoui, & Mars 1990), the “photometric redshift” method (Kodama, Bell, & Bower 1999), Voronoi tessellations (Ramella et al. 1998), and the “density morphology” relationship (Ostrander et al. 1998). The level of sophistication of these algorithms has increased in anticipation of high-quality CCD survey data, e.g., the Sloan Digital Sky Survey (SDSS) (Gunn et al. 1998).

The early automated catalogs of optically selected clusters have produced two important results. First, Postman et al. (1996) and Lumsden et al. (1992) both find evidence for a higher space density of clusters than that seen in the Abell catalog. For example, Postman et al. (1996) finds that the

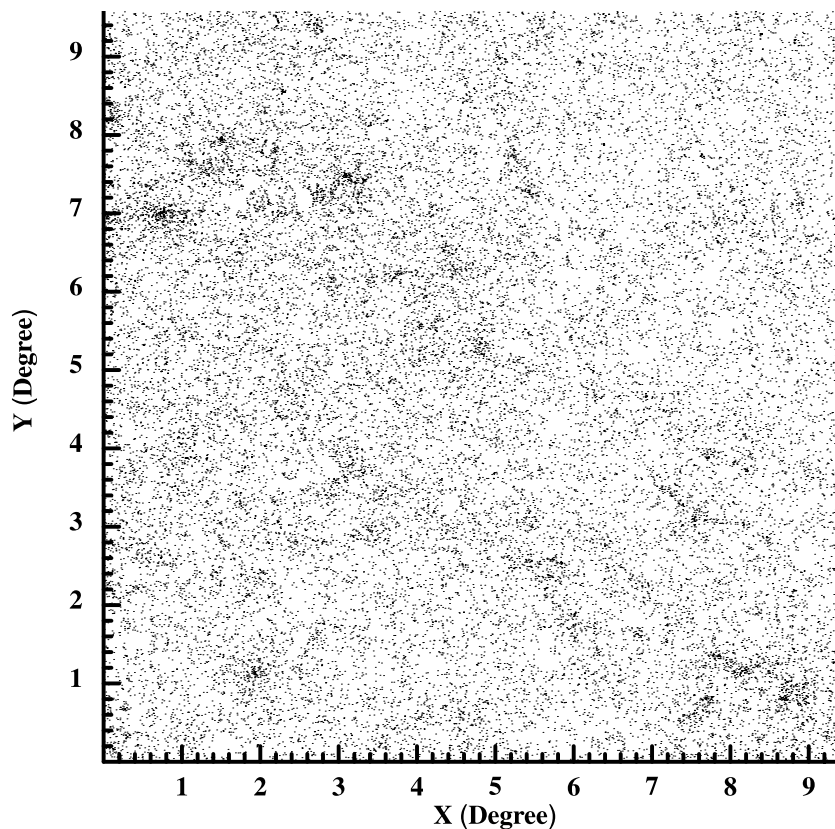


FIG. 1.—The  $10^\circ \times 10^\circ$  test region outlined in § 2 and used for our simulations. Cluster detections within  $5 \times \theta_c$  (at  $z = 0.05$  this is  $0.35^\circ$ ) of the edges of this data were discarded.

measured space density of clusters in the Palomar Distant Cluster Survey (PDCS) is a factor of  $5 \pm 2$  greater than that implied from the Abell catalog. Second, the space density of PDCS clusters remains constant between  $z = 0.2$  and  $z = 0.6$ , in agreement with the earlier work of Couch et al. (1991) and has been confirmed recently by Holden et al. (1999). If true, these results can be used to place strong constraints on the underlying galaxy evolution model (e.g., cold dark matter) and measurements of the cosmological parameters  $\sigma_8$  and  $\Omega_0$  (see Bahcall, Fan, & Cen 1997; Reichart et al. 1999; Holden et al. 1999).

To solidify these initial results, larger catalogs of clusters are required. Moreover, it is becoming increasingly clear that we need to compare these different cluster catalogs to help verify results and expand the redshift range over which we can study the cluster distribution. To date however, there has been little cross comparison between these different cluster catalogs. Foremost, the relationship between the X-ray and optical catalogs of clusters remains unclear (see Holden et al. 1997; Briel & Henry 1993; Bower et al. 1997). In the optical domain, different catalogs have used different cluster-finding algorithms, making it very difficult to cross calibrate catalogs and methods and thus verify results. This is illustrated by the fact that although both Lumsden et al. (1992) and Postman et al. (1996) find a higher space density than the Abell catalog, the PDCS finds 5 times as many clusters per unit volume, while the Edinburgh/Durham Cluster Catalogue (EDCC) (Lumsden et al. 1992) only finds twice as many clusters per unit volume as Abell. Therefore, it is impossible to fairly compare the EDCC and the PDCS

even though they are both objective, automated catalogs of clusters.

In this paper, we set out to rectify this problem by running a variant of the PDCS cluster-finding algorithm on the same galaxy data as used by Lumsden et al. (1992) in the construction of the EDCC. The main aim of this project is to provide a coherent set of cluster data that spans from  $z \sim 0.05$ , the lower redshift limit of the EDSGC, to  $z \simeq 0.6$ , the upper completeness limit of the PDCS. In addition to using a similar algorithm as Postman et al. (1996), we have performed a large number of Monte Carlo simulations to assess the completeness limit, and contamination rate, of this new EDCC cluster catalog. This is the first major application of the matched filter algorithm to low-redshift galaxy data; however, it is only the first of many such surveys presently under way, e.g., the SDSS, DeepRange (Postman et al. 1998), DPOSS (Gal et al. 2000), COSMOS (Schuecker & Boehringer 1998), and the CCD survey of Zaritsky et al. (1997).

In § 2, we discuss the EDSGC and the matched filter detection algorithm. In § 3, we outline the methodology used to detect our cluster candidates and discuss in detail the Monte Carlo simulations we performed to determine our detection thresholds, the effective area of our new cluster survey, and our spurious detection rate. Readers interested in just the results of this survey may wish to concentrate on § 4 of this paper, which presents our space density results. In § 5, we discuss these results in comparison with the PDCS and Abell cluster catalogs. Throughout this paper, we use  $H_0 = 100 h \text{ km s}^{-1} \text{ Mpc}^{-1}$  and  $q_0 = 0.5$  unless otherwise stated.

## 2. THE EDINBURGH/DURHAM SOUTHERN GALAXY CATALOGUE

The Edinburgh/Durham Southern Galaxy Catalogue (EDSGC) has been discussed in detail in Heydon-Dumbleton, Collins, & MacGillivray (1989), Lumsden et al. (1992), and Collins, Nichol, & Lumsden (1992), (2000). However, for consistency, we include here a brief discussion of the salient points of this catalog.

The whole EDSGC consists of 1.5 million galaxies brighter than  $b_j = 21.5$  covering an area of  $\sim 1100 \text{ deg}^2$  centered on the south Galactic pole, spanning  $90^\circ$  in right ascension and  $20^\circ$  in declination. The catalog is 95% complete to  $b_j = 20$  and has  $\leq 10\%$  stellar contamination. The catalog was constructed from COSMOS (a microdensitometer) scans of UK Schmidt IIIa-J photographic survey plates and as photometrically calibrated using 30 CCD sequences positioned in a “checkerboard fashion.” From the EDSGC, Lumsden et al. (1992) detected 733 galaxy overdensities using a simple “peak-finding” algorithm. Collins et al. (1995) present 777 redshifts measurements within 94 clusters, and this redshift sample has been used to study the large-scale distribution of nearby clusters (see Nichol et al. 1992; Guzzo et al. 1992; Martin et al. 1995) as well as the cluster luminosity function (Lumsden et al. 1997).

For the analysis discussion in § 3, we restrict ourselves to a small  $10^\circ \times 10^\circ$  random subregion of the EDSGC centered at  $00^{\text{h}}30^{\text{m}}$  in right ascension and  $-33^\circ$  in declination. We also restricted the magnitude range to  $15 < b_j < 20.5$  to remain as complete as possible (see Collins et al. 2000). These cuts resulted in a total of 41,171 galaxies, a number that is significantly smaller than the whole EDSGC. This test data is shown in Figure 1. For the space density results presented in § 4, we used all galaxies in the magnitude range  $15 < b_j < 20.5$  and in a coordinate range of  $22^{\text{h}} < \alpha < 3^{\text{h}}3$  and  $-42^\circ < \delta < -23^\circ$  ( $1067 \text{ deg}^2$ ), which gave us 627,260 galaxies in total.

We note here that the EDSGC has previously been used to construct an objective catalog of clusters of galaxies (see Lumsden et al. 1992). However, in this prior analysis, only a simplistic “peak-finding” algorithm was used to find candidate systems for redshift follow-up. Given the recent advances in cluster-finding algorithms, we decided it was prudent to repeat the analysis which we discuss herein. We stress, however, that this does not undermine the scientific integrity of the original EDCC (Lumsden et al. 1992) and results derived from it (Nichol et al. 1992; Collins et al. 1995; Martin et al. 1995). In this present work, we simply wish to analyze the low-redshift cluster population using the same techniques as presently used at high redshift (i.e., PDCS). For the sake of consistency, we call this new cluster catalog the Edinburgh/Durham Cluster Catalogue II (EDCCII).

## 3. METHODOLOGY

### 3.1. The Matched Filter

In recent years, there has been considerable progress in the development of new, automated cluster-finding algorithms (see Lumsden et al. 1992; Dalton et al. 1994; Postman et al. 1996; Kawasaki et al. 1998; Kepner et al. 1999; Schuecker & Boehringer 1998; Slezak et al. 1990; Kodama et al. 1999; Ramella et al. 1998; Ostrander et al. 1998). In this paper, we focus our attention on the matched filter algorithm since we are interested in directly comparing our results to those of Postman et al. (1996).

We have based our matched filter algorithm on the procedure outlined by Kawasaki et al. (1998), which compares the galaxy distribution around any point on the sky to a cluster model plus a background (see eq. [1] in Kawasaki et al. 1998). The parameters of this cluster model are given in equations (2), (3), and (4) of Kawasaki et al. (1998) and are the cluster surface density profile, the intrinsic richness of the cluster ( $N$  in eq. [1] of Kawasaki et al. 1998), the cluster and field luminosity functions, and the surface density of background galaxies ( $\sigma_f$ ). For the analysis discussed herein, we have modeled our clusters as a spherically symmetrical, isothermal surface density profile (i.e., a King profile with  $r_{\text{core}} = 170 \text{ kpc}$  and  $\beta = \frac{2}{3}$ ) combined with a Schechter luminosity function (with  $M_{b_j}^* = -20.12$  and  $\alpha = -1.25$ ; see Lumsden et al. 1997). The background galaxy distribution is modeled as a flat surface density of galaxies of  $\sigma_f = 583,775 \text{ galaxies sr}^{-1}$ , which is the measured average surface density of galaxies in the EDSGC in the magnitude range  $15 < b_j < 20.5$ . For the field luminosity function [ $\theta_f(m)$  in eq. (3) of Kawasaki et al. 1998], we used a Schechter function with  $M_{b_j}^* = -19.5$  and an  $\alpha = -1.1$  (see Loveday et al. 1992).

The physical model for the cluster plus background is converted to an observational model using the standard cosmological redshift-distance relationships (and  $k$ -corrections), and therefore the model is only a function of the intrinsic richness of the cluster and its redshift. This observed model is convolved with the data and a likelihood assigned for each point on the sky which is proportional to the quality of fit of the cluster model to the observed galaxy distribution given Poisson statistics (see eqs. [6] and [7] of Kawasaki et al. 1998). One can then maximize the likelihood by varying the two parameters of the model, i.e., richness and redshift. Computationally, this was achieved by overlaying the EDSGC with a grid (pixel scale of  $\theta_c/3$ ) and comparing each pixel, in this grid, with the matched filter model as a function of cluster redshift and richness ( $R_m$ ). For the results presented herein, we varied the matched filter redshift ( $z_{\text{est}}$ ) from 0.05 to 0.15 ( $\delta z_{\text{est}} = 0.0025$ ) and used richness estimates of  $R_m = 50, 100, 200, \text{ and } 400$ . This resulted in an array of likelihood and richness maps (see Kawasaki et al. 1998) from which we must select our cluster candidates.

### 3.2. Monte Carlo Simulations

In this section, we outline our Monte Carlo simulations which were used to determine the cluster detection thresholds as well as to estimate our spurious cluster detection rate and overall cluster detection efficiency.

#### 3.2.1. Model of a Cluster

For our Monte Carlo simulations, we must first create an artificial cluster. We used a spherically symmetrical, isothermal surface density profile with a cluster core radius ( $r_c$ ) of 170 kpc, a cutoff radius of  $5r_c$ , and a Schechter luminosity function with  $\alpha = -1.25$  and  $M_B^* = -20.12$  (we restricted ourselves to an absolute magnitude range of  $M_B^* \pm 5$ ). This artificial cluster was then redshifted appropriately using the standard cosmological relations and

$$m = M + (42.384 + 5 \log z) + (4.14z - 0.44z^2) \quad (1)$$

to convert absolute magnitude to apparent  $b_j$  magnitude (see Lumsden et al. 1997). To match the magnitude range covered by the EDSGC survey, we then removed all galaxies outside the magnitude range of  $15 < b_j < 20.5$ . Four

different intrinsic richnesses of artificial cluster were used in our Monte Carlo simulations:  $R_m = 50, 100, 200,$  and  $400$ . Unless otherwise stated, each artificial cluster was unique, with the galaxies distributed at random according to the angular and luminosity distributions given above.

We note here that no attempt was made to simulate the density-morphology relationship or to allocate a cD-type galaxy at the cluster core. Moreover, we did not change the shape or parameters of our artificial clusters during our simulations. Such simulations would have been computationally intensive but are clearly needed in the future.

### 3.2.2. Determination of the Thresholds

Crucial to any cluster-finding algorithm is the issue of threshold. As one changes the threshold above which a cluster is included in one's catalog, the resulting catalog of cluster candidates changes dramatically. The easiest way to determine such thresholds is via Monte Carlo simulations, i.e., by inserting artificial clusters into the real EDSGC data and attempting to maximize the number of detections of these artificial clusters.

Optimally, we wish to set the thresholds low enough to detect all our artificial clusters while minimizing the number of spurious detection. Therefore, the primary obstacle in determining the thresholds is the balance one must strike in maximizing the number of artificial clusters detected compared to the total number of clusters detected. This trade-off will ultimately be determined at the discretion of the authors; however, as long as we are consistent throughout our analysis, this should not undermine the objective nature of our cluster catalog.

We therefore inserted 20 artificial clusters into the EDSGC data at random locations and ran our cluster-finding algorithm on this data. We empirically determined that 20 clusters at one time was the maximum number of artificial clusters we could add to the data without skewing the statistics of the background galaxies; adding any more would have resulted in merging of the artificial clusters, while adding fewer clusters would have made the simulations laborious. We then varied the thresholds, both in richness (RT) and likelihood (LT), and computed for each combination the number of artificial clusters detected as well as the total number of clusters detected above these thresholds.

It was then necessary to weight these detections to determine the optimal thresholds. Clearly, we wish to rule out obvious cases, i.e., detecting one artificial cluster while detecting hundreds of other systems within the EDSGC (as most of these detections will be either lower richness clusters or spurious detections). Unfortunately, most cases we encountered were more subtle than this, i.e., detecting 10 artificial clusters within a total of 25 detections or detecting 15 artificial clusters within a total 40 detections. To help differentiate between these intermediate cases, we employed an analytical method which we outline below.

We defined the number of detections of our artificial clusters to be  $x$  and the number of total detections to be  $y$ . Both  $x$  and  $y$  are functions of RT and LT and increase with decreasing thresholds. We therefore defined a function  $[T(x, y)]$  which satisfied the following boundary conditions:  $T(0, y) = 0$ ,  $\lim_{y \rightarrow \infty} T(x, y) = 0$ , and the maximum of  $T(x, y)$  is at  $T(20, 20)$ . The functional form of  $T(x, y)$  is therefore important since it is now our weighting scheme. We estimated  $T(x, y)$  by running our cluster-finding algo-

TABLE 1  
RICHNESS THRESHOLD VALUES (RT) DETERMINED FOR  
VARIOUS REDSHIFTS AND CLUSTER RICHNESSES

$R_m$	REDSHIFT ( $z_{\text{est}}$ )				
	0.05	0.07	0.09	0.12	0.15
50.....	270	210	190	220	320
100.....	310	270	230	250	320
200.....	410	340	340	350	410
400.....	600	480	460	480	540

rithm over many thousands of realizations of our simulations and varying RT and LT to create a Monte Carlo estimate for  $T(x, y)$ . From these data, we empirically found that  $T(x, y) = x^3/y^{1.3}$  was the best functional form for this data and adopted it as our weighting scheme. Using this relationship, we then determined the optimal RT and LT thresholds as a function of redshift and intrinsic richness. Our thresholds are given in Tables 1 and 2 (we used linear interpolation between these values if necessary).

### 3.2.3. Locating Cluster Candidates

In this subsection, we review our procedure for identifying a unique cluster candidate above the thresholds outlined above. We first designate all pixels in our likelihood and richness maps that satisfy our thresholds,  $\geq \text{RT}$  and  $\geq \text{LT}$ , as "active" pixels. Obviously, a single cluster candidate will create multiple active pixels, so we must group these pixels together into single detection. This is achieved by searching for peaks in the distribution of active pixels, i.e., we look for an active pixel whose height is greater than any other active pixel within a radius of  $2\theta_c$  of the peak. We then group together all active points in this area to create a unique cluster candidate. If a single active pixel is a peak by default—i.e., there are no other active pixels within  $2\theta_c$  of it—we disregard this peak and do not include it in our final analysis. Such isolated peaks are unlikely to be caused by real clusters. Finally, we compute the weighted mean of all active points grouped together as a single cluster to determine the most likely cluster candidate centroid.

### 3.2.4. Determining Detection Efficiencies

In addition to determining our detection thresholds, our Monte Carlo simulations were used to estimate our detection efficiency and the effective area of our cluster search. This is an important aspect of any cosmological survey as it allows us to determine the volume sampled by the EDCCII

TABLE 2  
LOG LIKELIHOOD THRESHOLD VALUES (LT) DETERMINED FOR  
VARIOUS REDSHIFTS AND CLUSTER RICHNESSES

$R_m$	REDSHIFT ( $z_{\text{est}}$ )				
	0.05	0.07	0.09	0.12	0.15
50.....	-230	-130	-90	-65	-60
100.....	-230	-150	-90	-65	-65
200.....	-250	-160	-110	-80	-65
400.....	-360	-200	-140	-100	-70

and thus measure the space density of clusters from the catalog. Previous applications of automated optical cluster-finding algorithms have based their efficiency measurements on their ability to detect clusters within artificial galaxy data. For example, Postman et al. (1996) and Kepner et al. (1999) created artificial galaxy catalogs with the same statistical properties as real galaxy catalogs; e.g., they matched the surface density of galaxies and/or the large-scale clustering properties of the galaxies. They then added artificial clusters to such simulated galaxy data.

We, however, found this method inadequate since such simulated galaxy catalogs cannot fully reproduce the hierarchical structure of galaxies in the universe. Specifically, the effects of superpositions of structures, variations in the field counts, or large-scale structures are hard to include in these simulations. Therefore, for each combination of RT and LT (see Tables 1 and 2), we added a total of 6000 artificial clusters (20 at a time) at random in the EDSGC and computed our success rate in detecting these artificial clusters above our thresholds (an artificial cluster was considered detected if a candidate cluster was found by our algorithm within  $2\theta_c$  of the original coordinate of the artificial cluster;  $\theta_c$  was evaluated at the redshift of the artificial cluster).

In Figure 2, we present our average detection efficiencies as a function of input redshift and richness (using the  $10^\circ \times 10^\circ$  test area discussed in § 2 and in Fig. 1). The error bars are the standard deviation observed between the different trials of 20 clusters added to the EDSGC data at any one time.

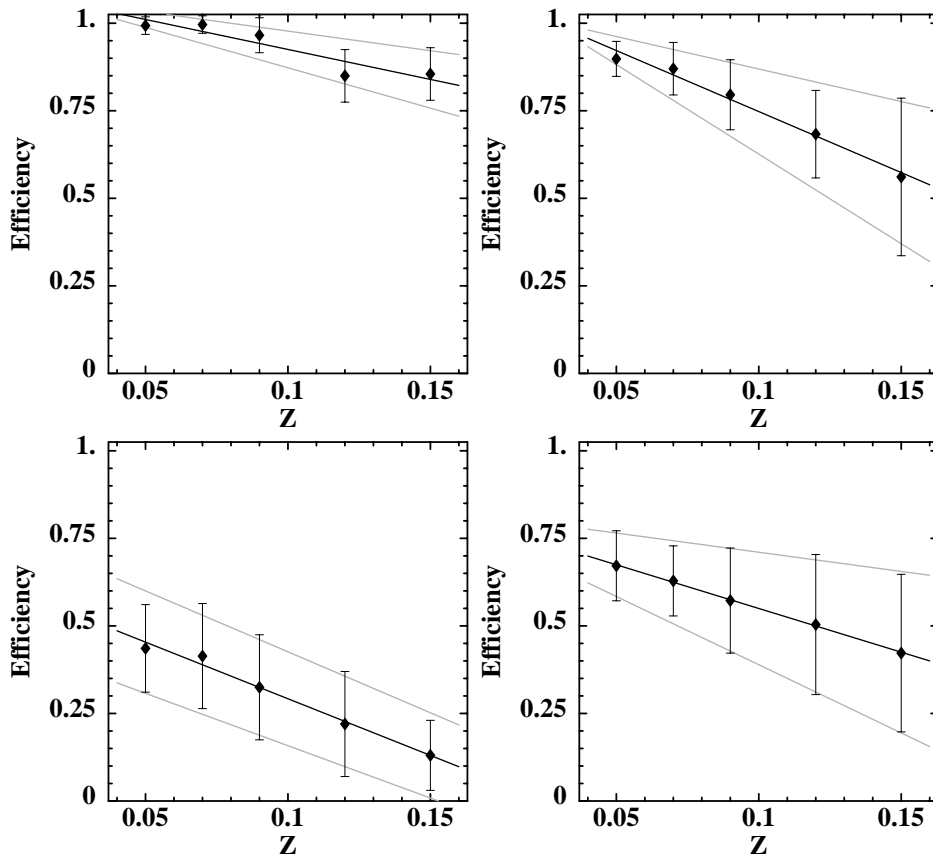


FIG. 2.—Average measured detection efficiency for clusters of various richness as a function of redshift. Clockwise from the upper left-hand panel, the graphs represent clusters of richnesses  $R_m = 400, 200, 100,$  and  $50$ .

In Figure 3, we show an example of the angular dependence of our detection efficiency. It is interesting to note that our efficiency is strongly correlated with the large-scale structure (LSS) in the universe. This effect is most prominent for lower richness clusters, while for the richer systems ( $R_m \geq 200$ ) it is insignificant (except at the highest redshifts probed by our simulations where the effect resulted in a loss of  $\approx 15\%$  of artificial clusters). In addition to this interference, our efficiency in detecting low-richness, high-redshift clusters was hindered by the magnitude limit of the EDSGC data since the number of potentially visible galaxies in these artificial clusters decreases below the noise in the background.

This problem of LSS interference appears to affect both over- and underdense regions of the EDSGC data (when compared to the mean surface density of galaxies). The most striking example of this LSS interference is seen at coordinates  $2^\circ 0', 7^\circ 5'$  in Figure 1, where a group of clusters—Abell 2730, 2721, 2749, 2755, and 12S—has reduced our detection efficiency to almost zero (see Fig. 3). In contrast, we also observe in Figure 3 a low detection efficiency near coordinates  $8^\circ 0', 6^\circ 0'$ , which coincides with an underdense region in Figure 1. We believe this effect is caused by our assumption of a flat, uniform galaxy background as used in the matched filter algorithm (see § 3.1). In both over- and underdense regions, our assumption of a flat background with the mean surface density of the EDSGC is poor, and therefore we suppress the overall likelihood of the cluster detection; i.e., the model of the background around the cluster is not a flat surface density of  $\sigma_f = 583,775$  galaxies  $\text{sr}^{-1}$ . This effect

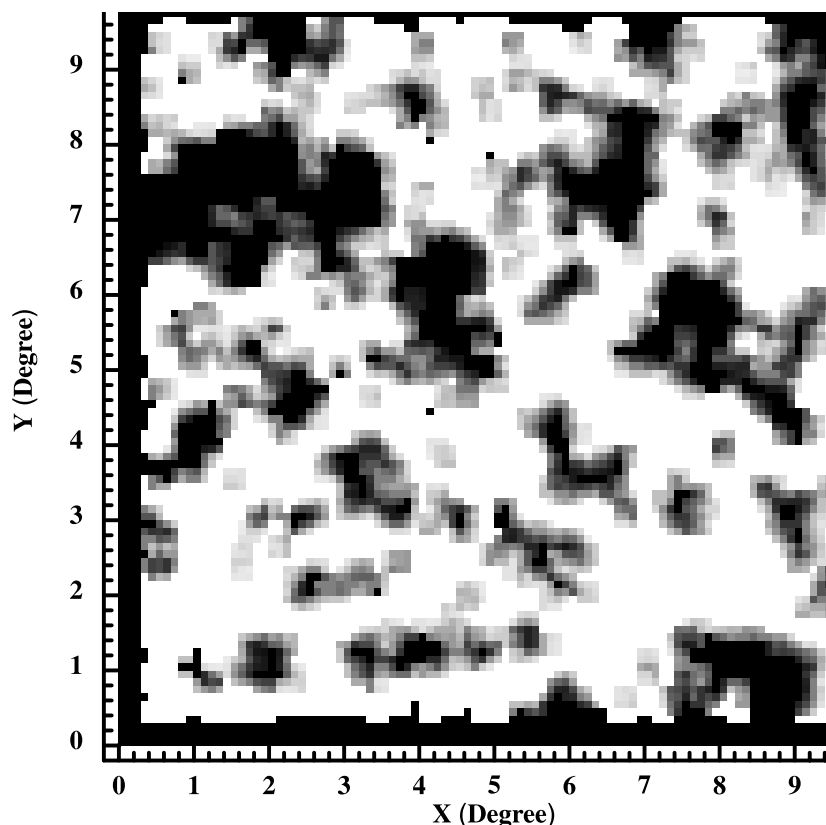


FIG. 3.—Our detection efficiency as a function of position in the EDSGC data shown in Fig. 1. Light areas indicate a detection efficiency of 100% for our artificial clusters, while dark areas indicate a 0% detection efficiency. Efficiencies near the edge of the area were not measured. This plot is for  $z_{\text{est}} = 0.05$  and  $R_m = 100$  artificial clusters.

is further exacerbated by systematic plate-to-plate uncertainties in the magnitude zero point of the EDSGC photographic plates (Nichol & Collins 1993).

We present the effective area of the whole EDCCII in Table 3 based on our simulation results. These data were obtained by summing over the larger EDSGC survey area, as defined in § 2, but weighted by our success rate in detecting artificial clusters as computed from the smaller test area. The data given in Table 3 illustrate the power of this new EDCCII catalog since we now know the selection function of an optically selected cluster catalog to the same accuracy as a X-ray-selected cluster survey (e.g., Nichol et al. 1999).

TABLE 3  
EFFECTIVE AREA ( $\text{deg}^2$ ) OF THE EDCCII AS A FUNCTION OF  
INPUT CLUSTER REDSHIFT AND RICHNESS

$R_m$	REDSHIFT ( $z_{\text{est}}$ ) ( $\text{deg}^2$ )				
	0.05	0.07	0.09	0.12	0.15
50 .....	580	516	415	266	196
100 .....	742	687	612	553	445
200 .....	962	928	855	729	594
400 .....	1067	1063	1034	966	908

NOTE.—These numbers were extrapolated from the efficiencies we derived for the smaller test area of the EDSGC.

This effective area will be used below when calculating the space density of clusters (see § 4).

### 3.2.5. Determining Spurious Detection Rate

The final use of our simulations was to determine the likely spurious detection rate. Again, we have tried to use the real galaxy data as much as possible in this analysis so as to mimic the real uncertainties in the EDSGC catalog. This is different from previous attempts to estimate the spurious detection rate which have relied on simulated galaxy catalogs (see Postman et al. 1996).

To achieve this goal, therefore, we perturbed each galaxy in the EDSGC in a random distance (between  $2\theta_c$  and  $5\theta_c$  with a flat distribution) in a random direction from its original position. This procedure effectively smoothes the galaxy catalog on these particular scales, removing all small-scale structure in the catalog while retaining the large-scale features within the catalog. We then applied our matched filter algorithm to these perturbed galaxy catalogs and calculated the number of clusters that would satisfy our selection criteria. This was performed many thousands of times to determine the standard deviation in our spurious detection rate.

Our spurious detection rates are shown in Figure 4. The number of spurious detections was significant only for high-redshift  $R_m = 50$  and  $R_m = 100$  clusters. Based on these simulations, therefore, we restrict ourselves to  $z \leq 0.12$  for  $R_m \leq 100$  and  $z \leq 0.15$  for  $R_m > 100$  to ensure that the spurious detection rate remains insignificant. For example, for

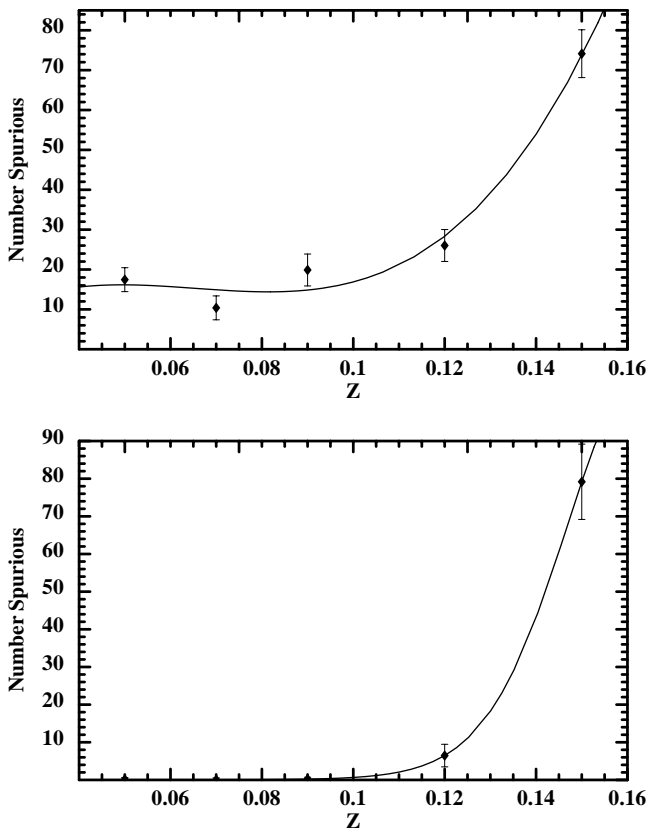


FIG. 4.—Number of spurious detections as a function of redshift for  $R_m = 50$  (top) and  $R_m = 100$  (bottom) clusters in our  $10^\circ \times 10^\circ$  EDSGC test area. Number of spurious detections for higher richness clusters were negligible, i.e., less than one spurious cluster in the  $10^\circ \times 10^\circ$  area.

$R_m \geq 200$  systems, less than 1% of detected clusters are likely to be spurious below  $z = 0.15$ . We also exclude all clusters at  $z < 0.05$  as our thresholds are not accurately calibrated below this redshift. In § 4, therefore, we restrict ourselves to  $R_m \geq 100$  systems in the redshift range  $0.05 < z < 0.15$  and make no correction for spurious detections within this richness and redshift range.

We note here that the results of these simulations are in good agreement with empirical determinations of the completeness of the EDSGC and EDCC; i.e., based on 777 galaxy redshift measurements, Nichol (1993) showed that the EDCC was complete out to  $z \simeq 0.13$  and only contained less than 15% contamination from spurious clusters. At low redshift, Lumsden et al. (1992) also had difficulty detecting  $z < 0.03$  clusters in the original EDCCI because of the large angular size subtended by such clusters.

In addition to randomizing the positions of the EDSGC, we also performed simulations which randomly shuffled the magnitudes of the galaxies throughout the EDSGC data. This resulted in galaxy catalogs with the same statistical properties—i.e., the same angular clustering and number-magnitude relationship—but removed all correlations with magnitude. Again, these randomized catalogs were analyzed with our matched filter algorithm and resulted in a very similar result as presented in Figure 4; i.e., the spurious detection rate was insignificant for lower redshift, higher richness systems. We note, however, that on average we detected fewer rich systems than with the real EDSGC data.

In other words, magnitude correlations only appear to aid in the detection of rich clusters in the data.

### 3.2.6. Merging of Catalogs

Once we have the cluster detections, as a function of redshift and richness, we must then remove duplicate cluster detections to produce a final catalog of unique cluster candidates. This was achieved by grouping together all systems whose measured centroids were within  $2 \times \theta_c$  of each other. We began this process by grouping together candidates as a function of their redshift, followed by their richness. If duplicates were found, we simply averaged their richness and redshift estimates to obtain a final estimate of the candidate clusters' richness and redshift.

## 4. THE SPACE DENSITY OF EDCCII CLUSTERS

In this section, we present the results of applying the matched filter algorithm as outlined in § 3 to the whole EDSGC (as defined in § 2). However, we must first establish a common framework within which to compare our results with previous studies. To this end, we will quote our results both as a function of  $\Lambda_{cl}$ , the cluster richness as defined by Postman et al. (1996) for the PDCS catalog and  $R_m$ , which is defined by us. As  $R_m$  and  $\Lambda_{cl}$  are just different richness normalizations of the matched filter model (see § 3.1), it is easy to relate the two analytically. This was achieved by integrating a normalized Schechter function of richness  $R_m$  over the luminosity range discussed in § 3.1 and dividing by  $L^*$ , the characteristic luminosity of the Schechter function. This is equivalent to the original definition of  $\Lambda_{cl}$  in Postman et al. (1996). Using  $\alpha = -1.1$  (Postman et al. 1996), we show that  $\Lambda_{cl} = 20.3$  is  $R_m = 100$ ,  $\Lambda_{cl} = 40.6$  is  $R_m = 200$ , and  $\Lambda_{cl} = 81.2$  is  $R_m = 400$ . We quote here  $\Lambda_{cl}$  in the PDCS  $V_4$  passband as this is closest to the EDSGC  $b_j$  passband.

In addition to comparing with the PDCS, we wish to compare with the original Abell catalog. We achieve this by combining the equality  $N_R(1.0)/N_R(1.5) \simeq 0.7$  (taken from Postman et al. 1996) with Figure 17 of Postman et al. (1996) to obtain an empirical relationship of  $R_{Abell} \sim 2 \times \Lambda_{cl}$  for low-redshift clusters ( $z \leq 0.2$ ). Therefore, the three  $\Lambda_{cl}$  richnesses given above approximately correspond to Abell richness classes (RC) 0, 1, and 2, respectively. These conversions are in good agreement with those presented in Lubin & Postman (1996) and references therein and used by others (B. Holden 1999, private communications; M. Postman 1999, private communications). For the rest of this paper, we concentrate on the  $R_m \geq 100$  systems ( $\Lambda_{cl} \geq 20$  or  $RC \geq 0$ ).

In Table 4, we present the cumulative surface densities of EDCCII clusters using the methodology outlined in this paper. To compute these surface densities, as a function of richness, we have summed the number of unique clusters with richnesses  $\geq R_m$ , divided by the effective areas in Table 3. The upper error bars quoted in Table 4 were computed by assuming all clusters detected at a particular richness are valid cluster candidates, i.e., if we count all clusters at that richness regardless of duplicate entries (see § 2). The lower error bars were computed using clusters only detected at that richness; i.e., they were not detected at any other  $R_m$  value. We note that these error bars are conservative and should be viewed as boundary values.

In Table 5, we present the EDCCII space densities along with cluster space density measurements from the PDCS,

TABLE 4  
COMPARISON OF CUMULATIVE SURFACE DENSITIES OF THE EDCCII AND THE PDCS

$R_m (\Lambda_{cl})$	$N [\geq R_m(\Lambda_{cl}), \leq z_{est}]$ (deg <sup>2</sup> )			
	0.12 or 0.15	0.3	0.4	0.6
$R_m \geq 100 (>20.3)$ .....	$0.41^{+0.72}_{-0.23} (z_{est} \leq 0.12)$	3.1	4.9	7.6
$R_m \geq 200 (>40.6)$ .....	$0.074^{+0.075}_{-0.029} (z_{est} \leq 0.15)$	1.4	3.2	5.9
$R_m \geq 400 (>81.2)$ .....	$0.015 \pm 0.015 (z_{est} \leq 0.15)$	0.015	0.4	1.4

NOTE.—The cumulative surface densities of the PDCS clusters were calculated using the data in Table 4 of Postman et al. 1996 using the EDCCII as a zero point. We excluded all PDCS clusters with  $\sigma < 3$  and a radius of more than 200 since such clusters have a higher probability of being spurious (see Postman et al. 1996). We assumed 5.1 deg<sup>2</sup> for the surface area of the PDCS survey. Our PDCS surface densities agree with those presented in Figure 21 of Postman et al. 1996. The EDCCII data presented in this table has not been corrected for spurious detections.

Holden et al. (1999), and the Abell catalog. For the EDCCII, we computed the space densities of clusters, as a function of richness  $[n(R_m)]$  using the formula

$$n(R_m) = \sum_{z_2}^{z_1} \frac{N(z_{est}, R_m)}{V(z) \times \Omega(R_m, z_{est})}, \quad (2)$$

which is a sum over all appropriate redshift slices ( $Z_{slices}$ ). Here,  $V(z)$  is the differential cosmological volume (per deg<sup>2</sup>),  $\Omega(R_m, z_{est})$  is the effective area as a function of redshift in Table 3,  $N(z_{est}, R_m)$  is the number of clusters detected within a redshift slice for a given richness  $R_m$ , and  $z_1$  and  $z_2$  are the limits of integration for the redshift slice. For  $R_m \leq 100$ , we have summed out to  $z_{est} = 0.12$ , while for  $R_m > 100$  we sum to  $z_{est} = 0.15$ . The error bars on these measurements were estimated using the same methodology as discussed above for the EDCCII cluster surface densities.

## 5. DISCUSSION

Recently, Holden et al. (1999) published 84 redshift measurements toward 16 low-redshift PDCS clusters. From these data, Holden et al. (1999) showed that the matched filter redshift estimate for  $z_{est} < 0.5$  PDCS clusters had an error of only  $\delta z \simeq 0.07$ , much smaller than previously quoted by Postman et al. (1996). Therefore, in Table 5 we present our estimates of the PDCS space density of low-redshift clusters ( $0.2 < z_{est} < 0.6$ ) using the PDCS  $z_{est}$  measurements and the data given in Table 4 of Postman et al. (1996). We have excluded all PDCS clusters with  $\sigma < 3$  and a radius of more than 200, in the  $V_4$  data, to minimize the effects of spurious detections (see Postman et al. 1996). Therefore, these space densities may be lower than expected since we have potentially excluded some real clusters as

well. This approach is valid as the true error on  $z_{est}$  is now significantly smaller than our redshift slice; i.e., a substantial number of clusters will not be scattered in, or out, of our sample because of the error in  $z_{est}$ .

For the  $40 \leq \Lambda_{cl} < 80$  ( $RC \sim 1$ ) clusters, we find good agreement between the PDCS and EDCCII space densities. The same can not be said for the  $RC \sim 0$  systems, where we differ by over an order of magnitude. We believe this discrepancy is the combination of two effects. First, the PDCS contains very few  $\Lambda_{cl} < 30$  clusters, indicating that the catalog is possibly incomplete at these low richnesses (the PDCS only contains seven such systems at these low richnesses). Secondly, the EDCCII may slightly overestimate the space density of low-richness clusters as the matched filter tends to deblend rich, nearby systems ( $z < 0.05$ ) into several lower richness clusters. Therefore, we will not discuss this inconsistency any further but note that this measurement will be important for the next generation of large-area CCD cluster surveys since they will possess the volume to probe the lower richness systems at high redshift. The EDCCII data will provide an important zero point for such surveys (DeepRange; Zaritsky et al. 1997). For  $RC \geq 2$  systems, the EDCCII appears to find a factor of  $\sim 4$  fewer clusters than the PDCS; however, the significance of this discrepancy is small given the (Poisson) errors on all measurements.

In addition to checking the matched filter redshift estimates, Holden et al. (1999) also computed the space density of PDCS clusters using a new, and completely independent, survey selection function than that used by Postman et al. (1996) and in this paper. Their results are presented in Table 5 and, within the errors, are in good agreement with both our PDCS and EDCCII space density measurements.

TABLE 5  
COMPARISON OF SPACE DENSITY MEASUREMENTS OF THE EDCCII, PDCS, AND ABELL CATALOGS

$n(R_m)$	CLUSTER SPACE DENSITIES ( $10^{-6} h^{-3} \text{Mpc}^{-3}$ )			
	EDCCII	PDCS	Holden et al. (1999)	Abell
$100 \leq R_m < 200 (\simeq 20 \leq \Lambda_{cl} < 40; RC \sim 0)$ .....	$83.5^{+193.2}_{-36.9}$	$6.9^{+6.1}_{-3.6}$	...	11.3
$200 \leq R_m < 400 (\simeq 40 \leq \Lambda_{cl} < 80; RC \sim 1)$ .....	$10.1^{+11.3}_{-4.3}$	$12.8^{+7.6}_{-5.0}$	$31.3^{+30.5}_{-17.1}$	4.04
$R_m \geq 400 (\simeq \Lambda_{cl} > 80; RC \geq 2)$ .....	$2.3^{+2.5}_{-2.3}$	$9.4^{+6.8}_{-4.7}$	$10.4^{+23.4}_{-8.4}$	1.58

NOTE.—The EDCCII space densities were calculated using eq. (1). The error bars for the EDCCII are discussed in the text, while we quote 68% error bars for the Holden et al. space densities as taken from their paper.

Moreover, Holden et al. 1999 (private communication) have recently recalculated their measurements of the PDCS space density, as given in Holden et al. (1999) and Table 5 but now based on a much larger sample of galaxy redshifts (over 700 redshifts in total). They now find  $\sim 18 \times 10^{-6} h^{-3} \text{Mpc}^{-3}$  for  $RC = 1$  systems and  $\sim 7 \times 10^{-6} h^{-3} \text{Mpc}^{-3}$  for  $RC \geq 2$  systems, which is closer to the EDCCII space densities presented in this paper.

In summary, we find good agreement among all three of these surveys (PDCS, Holden et al. 1999, and the EDCCII), which combined span a redshift range of  $0.05 \leq z \leq 0.6$ . At worst, the difference among the three surveys is  $4^{+10}_{-4}$  (Table 3). This therefore justifies our original desire to run the matched filter algorithm on the low-redshift EDSGC data since we are now comparing clusters selected in a similar way over this entire redshift range. We have thus removed one of the main uncertainties associated with the PDCS as we do not see a significant difference between the low- and high-redshift cluster populations (as originally highlighted by Postman et al. 1996). Moreover, this agreement implies that there is little evolution in the space density of optical clusters out to  $z \simeq 0.5$ , in agreement with results from X-ray surveys of clusters (see Nichol et al. 1997, 1999; Burke et al. 1997; Rosati et al. 1998; Vikhlinin et al. 1998; Ebeling et al. 1997, 2000). However, we should not overstate this claim, since the error bars on all measurements are large. In the future, we will need large samples of clusters that span a large range in redshift; this should be possible with the next generation of cluster catalogs constructed from surveys like DPOSS (Gal et al. 2000) and the SDSS (Gunn et al. 1998). We also urge the community to adopt one cluster-finding algorithm so it can be applied to different catalogs (at high and low redshift) consistently.

In Table 5, we present the space density of Abell clusters taken from Postman et al. (1996) and references therein. The EDCCII space density measurements appear to be systematically higher than the Abell catalog; e.g., we find  $\sim 7$  times as many  $RC \sim 0$  clusters as Abell. However, for  $RC > 0$  this discrepancy is much less, while the errors on these measurements are large. Therefore, we must be wary about overinterpreting any claimed discrepancy with Abell and simply note that overall the EDCCII has lessened the discrepancy previously claimed to be between the high- and low-redshift cluster populations.

Our potential disagreement with the Abell catalog could be due to two factors. First, like the EDCCII catalog, the effective area of the Abell catalog could be smaller than expected (see § 3). Second, the EDCCII could be finding more clusters than the Abell catalog at a given richness. The first of these two factors is hard to quantify given the subjective nature of the Abell catalog; however, the second factor can be addressed by cross-correlating individual clusters in

both the EDCCII and Abell catalogs. We discuss the latter below.

In total, we detect 182 of the 324 Abell clusters in the EDCCII area, or 56% of them (using a matching radius of 7.5). This is in good agreement with Lumsden et al. (1992) who find  $\sim 70\%$  match-up between their original EDCC clusters and the Abell catalog. In both cases, the percentage of match-ups is independent of richness; i.e., neither the EDCC or EDCCII appear to have missed Abell clusters of a particular richness class (see Fig. 8 of Lumsden et al.). In addition to comparing richnesses, we have also compared the distance estimates of our matched, and unmatched, Abell clusters and find little correlation. Therefore, the missing  $\sim 40\%$  of Abell clusters in the EDCCII catalog appear to be spread evenly over all richness and distance classes. Finally, for clusters in common between the EDCCII and Abell catalogs, we find no correlation between the two difference richness estimates, i.e.,  $R_m$  and Abell richness or RC. This agrees with Lumsden et al. (1992) and Postman et al. (1996), both of whom detect a large scatter between their richness estimates and the Abell richness estimates.

In contrast, there are a total of 2109 EDCCII clusters detected in the area given in § 2, a factor of  $\sim 8$  more than detected in the Abell catalog over the same area (we have excluded the supplementary Abell catalog here and in the above analysis). This discrepancy is lessened when we consider only  $R_m \geq 100$  systems where we find 227 EDCCII clusters (however, we note that the EDCCII only probes to  $z_{\text{est}} \leq 0.15$ , while the Abell catalog contains rich systems out to  $z \sim 0.4$ ). These raw numbers reflect the differences in the space densities measurements outlined in Table 5 and highlight that a vast majority of the new EDCCII systems are of lower richness (in the EDCCII catalog). Although, we do note that 143 of the 227  $R_m \geq 100$  systems (63%) are not in the Abell catalog (which corresponds to  $RC \geq 0$  systems). Again, these findings agree with the original EDCC cluster catalog where almost 70% of EDCC clusters were new compared to the Abell catalog. These two surveys therefore lend credence to the idea (already stated by Abell 1958 and Abell et al. 1989) that the Abell catalog should not be used for statistical studies.

The authors would like to thank Brad Holden, Lori Lubin, Adrian Pope, Marc Postman, and Kath Romer for their assistance during the course of this work. We also thank Chris Collins, Stuart Lumsden, Luigi Guzzo, and Harvey MacGillivray for allowing us free access to the EDSGC data. This project was funded through NASA grant NAG 5-3202 (R. C. N.) and two CMU Summer Undergraduate Research Grants (D. A. B.).

## REFERENCES

- Abell, G. O. 1958, *ApJS*, 3, 211  
 Abell, G. O., Corwin, H. G., Jr., & Olowin, R. P. 1989, *ApJS*, 70, 1  
 Bahcall, N. A., Fan, X., & Cen, R. 1997, *ApJ*, 485, L53  
 Bahcall, N. A., & Soneira, R. M. 1983, *ApJ*, 270, 20  
 Bower, R. G., Castander, F. J., Ellis, R. S., Couch, W. J., & Boehringer, H. 1997, *MNRAS*, 291, 353  
 Briel, U. G., & Henry, J. P. 1993, *A&A*, 278, 379  
 Burke, D. J., Collins, C. A., Sharples, R. M., Romer, A. K., Holden, B. P., & Nichol, R. C. 1997, *ApJ*, 488, L83  
 Collins, C. A., Guzzo, L., Nichol, R. C., & Lumsden, S. L. 1995, *MNRAS*, 274, 1071  
 Collins, C. A., Nichol, R. C., & Lumsden, S. L. 1992, *MNRAS*, 254, 295  
 ———. 2000, *ApJS*, submitted  
 Couch, W. J., Ellis, R. S., Maclaren, I., & Malin, D. F. 1991, *MNRAS*, 249, 606  
 Dalton, G. B., Efstathiou, G., Maddox, S. J., & Sutherland, W. J. 1992, *ApJ*, 390, L1  
 ———. 1994, *MNRAS*, 269, 151  
 de Grandi, S., et al. 1999, *ApJ*, 514, 148  
 Dodd, R. J., & MacGillivray, H. T. 1986, *AJ*, 92, 706  
 Ebeling, H., Edge, A. C., Fabian, A. C., Allen, S. W., Crawford, C. S., & Boehringer, H. 1997, *ApJ*, 479, L101

- Ebeling, H., et al. 2000, *ApJ*, 534, in press  
Gal, R. R., DeCarvalho, R. R., Odewahn, S. C., Djorgovski, S. G., Margoniner, V. E. 2000, *AJ*, 119, 12  
Gioia, I. M., Henry, J. P., Maccacaro, T., Morris, S. L., Stocke, J. T., & Wolter, A. 1990, *ApJ*, 356, L35  
Gunn, J. E., et al. 1998, *AJ*, 116, 3040  
Gunn, J. E., Hoessel, J. G., & Oke, J. B. 1986, *ApJ*, 306, 30  
Guzzo, L., Collins, C. A., Nichol, R. C., & Lumsden, S. L. 1992, *ApJ*, 393, L5  
Heydon-Dumbleton, N. H., Collins, C. A., & MacGillivray, H. T. 1989, *MNRAS*, 238, 379  
Holden, B. P., Nichol, R. C., Romer, A. K., Metevier, A., Postman, M., Ulmer, M. P., & Lubin, L. M., 1999, *AJ*, 118, 2002  
Holden, B. P., Romer, A. K., Nichol, R. C., & Ulmer, M. P. 1997, *AJ*, 114, 1701  
Jones, L. R., Scharf, C., Ebeling, H., Perlman, E., Wegner, G., Malkan, M., & Horner, D. 1998, *ApJ*, 495, 100  
Kawasaki, W., Shimasaku, K., Doi, M., & Okamura, S. 1998, *A&AS*, 130, 567  
Kepner, J., Fan, X., Bahcall, N., Gunn, J., Lupton, R., & Xu, G. 1999, *ApJ*, 517, 78  
Kodama, T., Bell, E. F., & Bower, R. G. 1999, *MNRAS*, 302, 152  
Kowalski, M. P., Cruddace, R. G., Wood, K. S., & Ulmer, M. P. 1984, *ApJS*, 56, 403  
Lidman, C. E., & Peterson, B. A. 1996, *AJ*, 112, 2454  
Loveday, J., Peterson, B. A., Efstathiou, G., & Maddox, S. J. 1992, *ApJ*, 390, 338  
Lubin, L. M., & Postman, M. 1996, *AJ*, 111, 1795  
Lumsden, S. L., Collins, C. A., Nichol, R. C., Eke, V. R., & Guzzo, L. 1997, *MNRAS*, 290, 119  
Lumsden, S. L., Nichol, R. C., Collins, C. A., Guzzo, L., 1992, *MNRAS*, 258, 1  
Martin, D. R., Nichol, R. C., Collins, C. A., Lumsden, S. A., & Guzzo, L. 1995, *MNRAS*, 274, 623  
Nichol, R. C. 1993, Ph.D. thesis, Univ. Edinburgh  
Nichol, R. C., & Collins, C. A. 1993, *MNRAS*, 265, 867  
Nichol, R. C., Collins, C. A., Guzzo, L., & Lumsden, S. L. 1992, *MNRAS*, 255, 21P  
Nichol, R. C., et al. 1999, *ApJ*, 521, L21  
Nichol, R. C., Holden, B. P., Romer, A. K., Ulmer, M. P., Burke, D. J., & Collins, C. A. 1997, *ApJ*, 481, 644  
Olsen, L. F., et al. 1999, *A&A*, 345, 681  
Ostrander, E. J., Nichol, R. C., Ratnatunga, K. U., & Griffiths, R. E. 1998, *AJ*, 116, 2644  
Postman, M., Huchra, J. P., & Geller, M. J. 1992, *ApJ*, 384, 404  
Postman, M., Lauer, T. R., Szapudi, I., & Oegerle, W., 1998, *ApJ*, 506, 33  
Postman, M., Lubin, L. M., Gunn, J. E., Oke, J. B., Hoessel, J. G., Schneider, D. P., & Christensen, J. A. 1996, *AJ*, 111, 615 (PDCS)  
Ramella, M., Nonino, M., Boschin, W., & Fadda, D., 1998, preprint (astro-ph/9810124)  
Reichart, D. E., Nichol, R. C., Castander, F. J., Burke, D. J., Romer, A. K., Holden, B. P., Collins, C. A., & Ulmer, M. P. 1999, *ApJ*, 518, 521  
Romer, A. K., et al. 1999, *ApJS*, accepted  
Rosati, P., Della Ceca, R., Norman, C., & Giacconi, R. 1998, *ApJ*, 492, L21  
Schuecker, P., & Bohringer, H. 1998, *A&A*, 339, 315  
Slezak, E., Bijaoui, A., & Mars, G. 1990, *A&A*, 227, 301  
Vikhlinin, A., McNamara, B. R., Forman, W., Jones, C., Quintana, H., & Hornstrup, A. 1998, *ApJ*, 502, 558  
Zaritsky, D., Nelson, A. E., Dalcanton, J. J., & Gonzalez, A. H. 1997, *ApJ*, 480, L91